Journal of Atmospheric Chemistry (2006) 53: 13–42
DOI: 10.1007/s10874-006-0948-0

A Numerical Model of the Partitioning of Trace Chemical Solutes during Drop Freezing

A. L. STUART[1] and M. Z. JACOBSON[2]

[1]*University of South Florida, 13201 Bruce B. Downs Blvd., MDC-56, Tampa, FL 33612, USA*
e-mail: astuart@hsc.usf.edu
[2]*Stanford University, Stanford, CA 94305-4020, USA*
e-mail: jacobson@stanford.edu

(Received: 31 March 2005; accepted: 6 July 2005)

Abstract. Partitioning of volatile chemicals among the gas, liquid, and solid phases during freezing of liquid water in clouds can impact trace chemical distributions in the troposphere and in precipitation. We describe here a numerical model of this partitioning during the freezing of a supercooled liquid drop. Our model includes the time-dependent calculation of the coupled processes of crystallization kinetics, heat transport, and solute mass transport, for a freezing hydrometeor particle. We demonstrate the model for tracer partitioning during the freezing of a 1000 μm radius drop on a 100 μm ice substrate, under a few ambient condition scenarios. The model effectively simulates particle freezing and solute transport, yielding results that are qualitatively and quantitatively consistent with previous experimental and theoretical work. Results suggest that the ice shell formation time is governed by heat loss to air and not by dendrite propagation, and that the location of ice nucleation is not important to freezing times or the effective partitioning of chemical solutes. Even for the case of nucleation at the center of the drop, we found that dendrites propagated rapidly to form surface ice. Freezing then proceeded from the outside in. Results also indicate that the solid-liquid interfacial surface area is not important to freezing times or the effective partitioning of chemical solutes, and that the rate aspects of trapping are more important than equilibrium solid-liquid partitioning to the effective partitioning resulting from freezing.

Key words: chemical retention, clouds, scavenging, ice, precipitation

1. Introduction

Convective clouds impact tropospheric chemistry through transport and transformation of trace chemical species. Through scavenging of chemical species, they contribute to acid deposition (Hales and Dana, 1979). They also transport and mix trace species between the atmospheric boundary layer and the upper troposphere (e.g. Chatfield and Crutzen, 1984; Dickerson *et al.*, 1987). Hence, they have important impacts on the global nitrogen budget (e.g. Logan, 1983), and on upper tropospheric concentrations of ozone (e.g., Pickering *et al.*, 1992) and odd hydrogen (Prather and Jacob, 1997; Jaegle *et al.*, 1997). Despite the presence of ice in many cloud systems, interactions between trace chemicals and ice are not well

understood (Abbatt, 2003). Here, we focus on studying partitioning of chemical solutes between the air, liquid water, and ice phases during freezing of supercooled drops.

Chemical solutes originally dissolved in a supercooled drop may be retained or expelled from the drop as it freezes. Research indicates that non-volatile species, such as sulfate, are efficiently retained during freezing (e.g., Mitchell and Lamb, 1989). However, the overall partitioning of more volatile species resulting from freezing (here termed 'effective partitioning') is not well characterized. Several laboratory and field studies have measured effective partitioning ratios ('retention' ratios) for soluble gases found in clouds, including H_2O_2, SO_2, O_2, HCl, NH_3, and HNO_3, HCOOH, and CH_3COOH (e.g. Lamb and Blumenstein, 1987; Iribarne and Pyshnov, 1990; Snider *et al.*, 1992; Voisin *et al.*, 2000). The retention ratio is defined as the ratio of solute mass in the hydrometeor particle after freezing to the mass originally dissolved in the drop. Measured retention ratios range widely from approximately 0.01 to 1. Several studies have investigated the dependence of retention ratio on freezing conditions. Correlations of the retention ratio with drop temperature, drop pH, ventilation rate, accretion rate, and drop impact velocity were found (Lamb and Blumenstein, 1987; Iribarne *et al.*, 1990; Snider *et al.*, 1992; Iribarne and Barrie, 1995; Snider and Huang, 1998). However, apparently contradictory results among studies have left significant uncertainty in the applicability of these findings to the variety of freezing conditions in natural clouds. Nonetheless, cloud modeling studies have found that partitioning of solutes during hydrometeor freezing may significantly affect chemical distributions in the troposphere and deposition to the ground (Cho *et al.*, 1989; Chen and Lamb, 1990; Wang and Chang, 1993; Audiffren *et al.*, 1999; Mari *et al.*, 2000; Barth *et al.*, 2001; Yin *et al.*, 2002).

A better understanding of the partitioning of volatile chemical solutes during freezing is needed in order to quantify its effects on tropospheric gas-phase and precipitation chemistry. In previous work (Stuart and Jacobson, 2003, 2004), we used time scaling analyses to provide a basic understanding of the dependence of the effective partitioning on chemical properties and freezing conditions and to predict retention ratios for a variety of conditions and chemicals. We found effective partitioning to be highly chemical specific and dependent on the Henry's constant of the solute, the pH, temperature, drop size, and ventilation conditions. Predicted retention ratios compared well with much of the experimental data, but not all. To elucidate better the complex, coupled, non-steady process interactions involved in the partitioning of volatile chemical solutes during freezing, we have developed a drop-scale numerical model. Here, we discuss the model physics and mathematical representation, and demonstrate its use.

2. Development of Model Equations

Our numerical model represents the coupled heat transport and solute mass transport processes that occur during freezing in a spherical solute-containing liquid

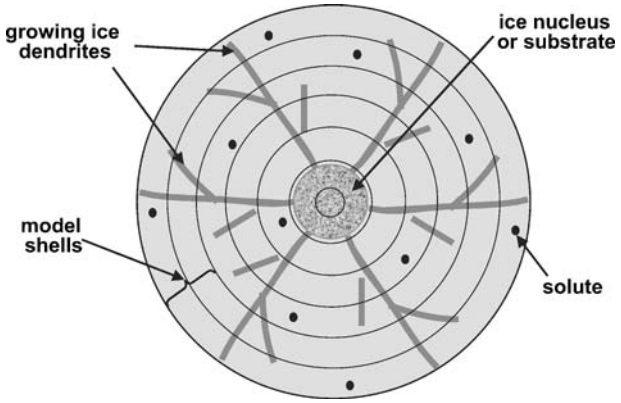

Figure 1. An idealized depiction of the numerical model. The model domain is made up of spherical shells. A supercooled drop is assumed to spread evenly around an ice nucleus or accretion substrate, which initiates freezing. Each model shell is made up of a volume fraction of ice and fraction of liquid water, to represent the dendritic character of ice crystal growth in supercooled drops.

hydrometeor particle with a accretion substrate or ice nucleus (which are collectively referred to here as an 'ice substrate') at its center. Figure 1 provides an idealized depiction of hydrometeor particle freezing, which was used to formulate our model. Model calculations are initiated at freezing nucleation (we do not consider ice nucleation rates here). At time 0, a supercooled drop is assumed to be spread evenly around the ice substrate. The size of the drop and the ice substrate are specifiable. As time progresses, the drop freezes and solute is expelled at rates governed by both the grid-resolved radial heat transport and solute mass transport processes, and the subgrid-scale processes occurring at the solid-liquid interface. To couple the grid-resolved and subgrid-scale processes, and to represent the dendritic character of drop freezing, we treat the solid-liquid interface as a 'mushy zone' (after Tien and Geiger, 1967). With this treatment, phase changes in each radial shell provide a volume source of sensible heat and mass to the water phases in the shell. Model calculations terminate when all liquid water has frozen.

2.1. GRID-RESOLVED PROCESSES

Figure 2 illustrates the processes that are resolved on the model grid. Each radial model shell can consist of both ice and liquid water, such that the amount of each is represented by a volume fraction. F_s is the volume fraction of (solid) ice and F_l $(=1 - F_s)$ is the volume fraction of liquid water in any shell. Within each shell, there is an average temperature for each phase, T_s and T_l, and an average concentration of any given solute for each phase, C_s and C_l.

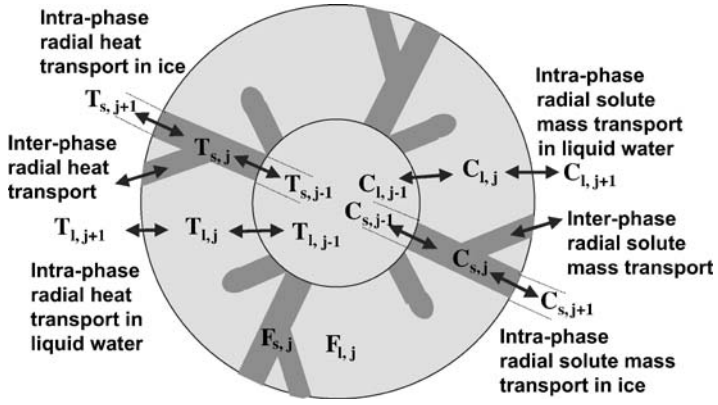

Figure 2. Processes resolved at the grid scale. For each shell there are average volume fractions of ice and liquid water (F_s and $F_l = 1 - F_s$), an average temperature in each phase (T_s and T_l), and an average solute concentration in each phase (C_s and C_l). Grid-scale processes include intra- and inter-phase radial heat and solute mass transport.

2.1.1. *Radial Heat Transport*

To develop equations for the radial heat transport, an energy balance over a spherical radial shell was performed for each phase of water (liquid and solid). For the liquid phase, this takes the form

$$\dot{Q}_{a-l} = \dot{Q}_{c-ll} + \dot{Q}_{c-\mathrm{int}} \tag{1}$$

where $\dot{Q}_{a-l}$ is the accumlation of energy (e.g. in units of J/s) in liquid water in the shell over a time step, Δt. $\dot{Q}_{c-ll}$ is the intra-phase (liquid-liquid) conduction of energy across the shell boundaries, and $\dot{Q}_{c-\mathrm{int}}$ is the inter-phase (liquid-solid) conduction of energy across the shell boundaries. Convection is not explicitly treated, but its effects can be included through the use of an effective conductivity. Viscous energy dissipation and radiative energy transport are also neglected. We further assume that the densities of liquid water and ice are constant and equivalent.

Energy accumulation is given by

$$\dot{Q}_{a-l} = \rho_l c_l \frac{\partial T_l}{\partial t} F_l 4\pi r^2 \Delta r \tag{2}$$

where ρ_l is the density of liquid water, c_l is the specific heat of liquid water at constant pressure, T_l is the absolute temperature of liquid water in the shell, r is the radial distance in the shell from the center of the sphere, and Δr is the shell radial thickness.

Liquid-liquid intra-phase inter-shell heat transport is given by

$$\dot{Q}_{c-\mathrm{ll}} = -\kappa_l \frac{\partial T_l}{\partial r} F_l 4\pi r^2|_r + \kappa_l \frac{\partial T_l}{\partial r} F_l 4\pi r^2|_{r+\Delta r} \tag{3}$$

where κ_l is the thermal conductivity of liquid water. At the shell edge, F_l is a surface area fraction of liquid water.

Liquid-solid inter-phase inter-shell heat transport is given by

$$\dot{Q}_{c-\text{int}} = -\kappa_{\text{int}} \frac{\partial T_{\text{int}}}{\partial r} F_{\text{int}} 4\pi r^2|_r + \kappa_{\text{int}} \frac{\partial T_{\text{int}}}{\partial r} F_{\text{int}} 4\pi r^2|_{r+\Delta r} \tag{4}$$

where F_{int} is the fractional interfacial surface area at the shell edge and $-\kappa_{\text{int}} \frac{\partial T_{\text{int}}}{\partial r}$ is the inter-phase energy flux. κ_{int} is modeled by treating the inter-phase heat transport process with two-film (resistance) theory (e.g. Sherwood *et al.*, 1975), for which $\kappa_{\text{int}} = \kappa_s \kappa_l / (\kappa_s + \kappa_l)$ and κ_s is the thermal conductivity of ice.

Substituting these heat transport terms into the energy balance (Equation (1)), results in the following grid-scale partial differential equation for radial heat transport for liquid water:

$$F_l \rho_l c_l \frac{\partial T_l}{\partial t} = \frac{1}{r^2} \frac{\partial}{\partial r} \left[r^2 F_l \kappa_l \frac{\partial T_l}{\partial r} \right] + \frac{1}{r^2} \frac{\partial}{\partial r} \left[r^2 F_{\text{int}} \kappa_{\text{int}} \frac{\partial T_{\text{int}}}{\partial r} \right] \tag{5}$$

For ice, the grid-scale radial heat transport differential equation is

$$F_s \rho_s c_s \frac{\partial T_s}{\partial t} = \frac{1}{r^2} \frac{\partial}{\partial r} \left[r^2 F_s \kappa_s \frac{\partial T_s}{\partial r} \right] + \frac{1}{r^2} \frac{\partial}{\partial r} \left[r^2 F_{\text{int}} \kappa_{\text{int}} \frac{\partial T_{\text{int}}}{\partial r} \right] \tag{6}$$

2.1.2. *Radial Solute Mass Transport*

Differential equations for solute mass transport in each phase can be derived similarly, using a shell mass balance approach. The resulting equations are

$$F_l \frac{\partial C_l}{\partial t} = \frac{1}{r^2} \frac{\partial}{\partial r} \left[r^2 F_l D_l \frac{\partial C_l}{\partial r} \right] + \frac{1}{r^2} \frac{\partial}{\partial r} \left[r^2 F_{\text{int}} \left(D_{\text{int}} \frac{\partial C_{\text{int}}}{\partial r} \right)_l \right] \tag{7}$$

$$F_s \frac{\partial C_s}{\partial t} = \frac{1}{r^2} \frac{\partial}{\partial r} \left[r^2 F_s D_s \frac{\partial C_s}{\partial r} \right] + \frac{1}{r^2} \frac{\partial}{\partial r} \left[r^2 F_{\text{int}} \left(D_{\text{int}} \frac{\partial C_{\text{int}}}{\partial r} \right)_s \right] \tag{8}$$

where C_l and C_s are the solute concentrations in liquid water and ice, respectively. D_l, D_s, and D_{int} are the solute diffusivities in liquid water, in ice, and across the solid-liquid interface, respectively. D_{int} can be modeled using two-film theory, similarly to κ_{int}, but we must account for the (dimensionless) equilibrium solid-liquid distribution coefficient, H_{sl} (i.e. the concentration of solute in ice versus that in liquid water, at equilibrium). Equating fluxes between phases yields $(D_{\text{int}})_l = H_{sl}(D_{\text{int}})_s$. Additionally, $\frac{(\partial C_{\text{int}})_l}{\partial r}$ and $\frac{(\partial C_{\text{int}})_s}{\partial r}$ can be discretized as $(C_l|_j - C_s|_{j-1}/H_{sl})/\Delta r$ and $(C_s|_j - H_{sl} C_l|_{j-1})/\Delta r$, respectively, where j is the radial shell index. However, model computations currently neglect grid-scale radial inter-phase mass transport, and it is treated only at the subgrid scale.

2.1.3. *Boundary Conditions*

To solve the above equations, boundary conditions are needed. At the center of the grid ($r = 0$), mass and energy conservation requires all fluxes to be zero, i.e.:

$$-\kappa_s \frac{\partial T_s}{\partial r} = -\kappa_l \frac{\partial T_l}{\partial r} = -\kappa_{\text{int}} \frac{\partial T_{\text{int}}}{\partial r} = 0 \tag{9}$$

$$-D_s \frac{\partial C_s}{\partial r} = -D_l \frac{\partial C_l}{\partial r} = -D_{\text{int}} \frac{\partial C_{\text{int}}}{\partial r} = 0 \tag{10}$$

At the particle-air boundary ($r = R$, where R is the particle radius), heat transport to/from air is represented by a first-order rate equation that accounts for energy loss due to convectively enhanced heat conduction and evaporation/sublimation (Macklin and Payne, 1967):

$$-\kappa_l \frac{\partial T_l}{\partial r} = \frac{1}{R}\left[\kappa_a G_h (T_l - T_a) + L_e D_v G_m \left(\frac{P_{\text{sat}}^{v,l}}{R_v T_l} - \frac{p_a}{R_v T_a}\right)\right] \tag{11}$$

$$-\kappa_s \frac{\partial T_s}{\partial r} = \frac{1}{R}\left[\kappa_a G_h (T_s - T_a) + L_s D_v G_m \left(\frac{P_{\text{sat}}^{v,s}}{R_v T_s} - \frac{p_a}{R_v T_a}\right)\right] \tag{12}$$

where T_a is the temperature of air, p_a is the partial pressure of water vapor in air, κ_a is the thermal conductivity of air, D_v is the diffusivity of water vapor in air, G_h and G_m are the ventilation coefficients for gas-phase heat and (water vapor) mass transport, L_e and L_s are the latent heats of evaporation and sublimation, $P_{\text{sat}}^{v,l}$ and $P_{\text{sat}}^{v,s}$ are the saturation vapor pressures of water vapor over liquid water and over ice, and R_v is the gas constant for water vapor (i.e, the universal gas constant divided by the molecular weight of water).

For solute mass transport, the particle-air boundary conditions were represented as

$$-D_l \frac{\partial C_l}{\partial r} = K_{mt}^{lg}(C_l - C_a H_{lg}) \tag{13}$$

$$-D_s \frac{\partial C_s}{\partial r} = K_{mt}^{sg}(C_s - C_a H_{sg}) \tag{14}$$

where C_a is the concentration of solute in air. H_{lg} is the (dimensionless) Henry's constant in terms of liquid-phase concentration over gas-phase concentration. $H_{lg} = K_h R_g T$, where K_h is the dimensional (e.g. M/atm) Henry's constant, R_g is the universal gas constant, and T is the absolute temperature. $H_{sg} = H_{lg} H_{sl}$ is the solute solid-gas distribution coefficient. The overall liquid-gas and solid-gas mass transfer coefficients, K_{mt}^{lg} and K_{mt}^{sg}, were developed from two-film theory (Sherwood *et al.*, 1975). They are given by

$$K_{mt}^{lg} = \frac{k_{mt}^{l} k_{mt}^{g} / H_{lg}}{k_{mt}^{l} + k_{mt}^{g} / H_{lg}} \tag{15}$$

$$K_{mt}^{sg} = \frac{k_{mt}^{s} k_{mt}^{g} / H_{sg}}{k_{mt}^{s} + k_{mt}^{g} / H_{sg}} \tag{16}$$

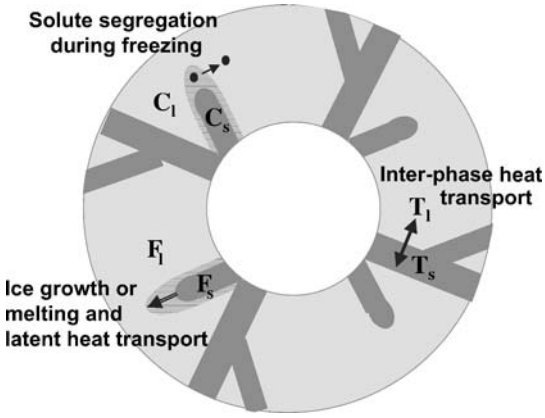

Figure 3. Processes treated at the subgrid scale. Subgrid-scale processes include ice crystal growth or melting, latent heat transport, inter-phase heat transport, and solute segregation during freezing (inter-phase mass transport).

where k^s_{mt}, k^l_{mt}, and k^g_{mt} are the local solid-, liquid-, and gas-phase solute mass transfer coefficients. $k^s_{mt} = 2\pi^2 D_s/\Delta r$, $k^l_{mt} = 2\pi^2 D_l/\Delta r$, and $k^g_{mt} = G_m D_g/R$, where D_g is the solute diffusivity in air and G_m is the ventilation coefficient for gas-phase mass transport (of solute).

2.2. SUBGRID-SCALE PROCESSES

Processes represented at the subgrid scale include freezing, latent heat transport, inter-phase heat transport, and inter-phase solute mass transport during freezing. Figure 3 illustrates these processes.

2.2.1. *Freezing*

In each shell, we determine volume freezing by a kinetic equation for ice crystal growth, such that

$$\frac{\partial F_s}{\partial t} = A_v b_1 (\Delta T_{\text{int}})^{b_2} \tag{17}$$

where $b_1(\Delta T_{\text{int}})^{b_2}$ is the intrinsic crystal interface growth speed, v. To obtain a volume fraction phase change due to freezing, we multipy the interfacial growth speed by the specific solid-liquid interfacial area in the shell, A_v. For simulations, we estimate A_v as the ratio of the shell surface area to its volume, $1/\Delta r$. $\Delta T_{\text{int}} = T_o - T_{\text{int}}$ is the supercooled temperature of the solid-liquid interface, where T_o is the equilibrium freezing temperature of water (0 °C) and T_{int} is the interface temperature. We estimate T_{int} as the average of the phase-specific temperatures in the shell, or $(T_s + T_l)/2$.

The form of the ice growth speed equation and the pre- and post-exponential factors (b_1 and b_2) are based on experimental data and theory for growth rates of ice in supercooled water (e.g. Pruppacher and Klett, 1997). For $0 < \Delta T_{\text{int}} \leq 10$ (K or °C), we use b_1 of 0.3 and b_2 of 2 (Bolling and Tiller, 1961). For $\Delta T_{\text{int}} > 10$, we use a b_1 of 2.3 and b_2 of 1 (Pruppacher and Klett, 1997, p. 674). If $\Delta T_{\text{int}} < 0$, Equation 17 is also used to calculate melting rates, with $\frac{\partial F_s}{\partial t}$ given opposite sign.

2.2.2. *Latent Heat Transport*

Freezing is a source of sensible heat to the shell. To account for this source we need to distribute the released heat into the ice and liquid water phases. To ensure enthalpy conservation, we use an integral equation to solve for temperature changes due to released latent heat of fusion. An enthalpy balance over a shell for an incremental freezing time step results in

$$M_l^f \left[\int_{T_b}^{T_l^f} c_s \mathrm{d}T + L_m|_{T_l^f} \right] + M_s^f \int_{T_b}^{T_s^f} c_s \mathrm{d}T = M_l^i \left[\int_{T_b}^{T_l^i} c_s \mathrm{d}T + L_m|_{T_l^i} \right] + M_s^i \int_{T_b}^{T_s^i} c_s \mathrm{d}T \tag{18}$$

where M represents mass of water (as solid or liquid). Subscripts on M and T describe the phase (l for liquid water and s for solid ice) and superscripts describe whether it is the value prior to (i for initial) or after (f for final) the freezing time step. T_b is an arbitrary base state temperature, which is assumed to be ice, and L_m is the latent heat of fusion.

Substituting for M_l and M_s with $\rho_l F_l V$ and $\rho_s F_s V$, where V is the shell volume, and assuming $\rho_l = \rho_s$, leads to the integral balance:

$$F_l^f \left[\int_{T_b}^{T_l^f} c_s \mathrm{d}T + L_m|_{T_l^f} \right] + F_s^f \left[\int_{T_b}^{T_s^f} c_s \mathrm{d}T \right] = F_l^i \left[\int_{T_b}^{T_l^i} c_s \mathrm{d}T + L_m|_{T_l^i} \right] + F_s^i \left[\int_{T_b}^{T_s^i} c_s \mathrm{d}T \right] \tag{19}$$

Since Equation (19) is underdetermined, we must make an additional assumption in order to solve for temperatures. Hence, we assume that the final temperatures in both phases in the shell are equal immediately after a freezing step.

Equation (19) includes integrals whose limits are the unknowns (the final temperatures of ice and liquid water). Hence, it must be solved iteratively. This is computationally costly. Therefore, we also developed an approximate difference equation. We again start with an enthalpy balance for freezing, of the form

$$\Delta H = \Delta H_l + \Delta H_s = 0 \tag{20}$$

where ΔH is the overall enthalpy change, and ΔH_l and ΔH_s are the enthalpy changes in liquid water and (solid) ice, respectively. Since enthalpy is a thermodynamic state function, we can represent the enthalpy change due to freezing with any path of processes. We represent the enthalpy change of liquid water with the following sequence: (1) a mass change to the final mass of liquid water at constant initial temperature ($\Delta H_{dM,M_l^f}|_{T_l^i}$) and (2) a temperature change to the final temperature of liquid water at constant final mass ($\Delta H_{dT,T_l^f}|_{M_l^f}$). We represent the enthalpy change of ice with the following sequence: (1) a temperature change to the initial liquid water temperature at constant initial mass ($\Delta H_{dT,T_l^i}|_{M_s^i}$); (2) a mass change to the final mass of ice at constant (inital liquid water) temperature ($\Delta H_{dM,M_s^f}|_{T_l^i}$); (3) a temperature change back to the initial temperature of ice, at constant final mass ($\Delta H_{dT,T_s^i}|_{M_s^f}$); and (4) a temperature change to the final temperature of ice at constant final mass ($\Delta H_{dT,T_s^f}|_{M_s^f}$). Using this path, we get:

$$\Delta H_l = \Delta H_{dM,M_l^f}|_{T_l^i} + \Delta H_{dT,T_l^f}|_{M_l^f} \tag{21}$$

$$\Delta H_s = \Delta H_{dT,T_l^i}|_{M_s^i} + \Delta H_{dM,M_s^f}|_{T_l^i} + \Delta H_{dT,T_s^i}|_{M_s^f} + \Delta H_{dT,T_s^f}|_{M_s^f} \tag{22}$$

Combining these with Equation (20) and rearranging yields

$$\begin{aligned} 0 = {} & \Delta H_{dM,M_l^f}|_{T_l^i} + \Delta H_{dM,M_s^f}|_{T_l^i} + \Delta H_{dT,T_l^f}|_{M_l^f} + \Delta H_{dT,T_s^f}|_{M_s^f} \\ & + \Delta H_{dT,T_l^i}|_{M_s^i} + \Delta H_{dT,T_s^i}|_{M_s^f} \end{aligned} \tag{23}$$

For small changes in mass (small enough time steps), $\Delta H_{dM,M_l^f}|_{T_l^i}$ and $\Delta H_{dM,M_s^f}|_{T_l^i}$ can be approximated by $(\frac{\partial H}{\partial M})_l \Delta M_l$ and $(\frac{\partial H}{\partial M})_s \Delta M_s$, respectively. Since $L_m = (\frac{\partial H}{\partial M})_l - (\frac{\partial H}{\partial M})_s$ and $\Delta M_l = -\Delta M_s$, the first two terms in Equation (23) sum to $-L_m|_{T_l^i}\Delta M$, where $\Delta M = M_s^f - M_s^i$. For small changes in liquid water or ice temperature, $\Delta H_{dT,T_l^f}|_{M_l^f}$ and $\Delta H_{dT,T_s^f}|_{M_s^f}$ can be approximated by $M_l^f c_l \Delta T_l$ and $M_s^f c_s \Delta T_s$, respectively. Since the difference between the initial liquid water and ice temperatures does not decrease with decreasing time step, the integral over temperature in the last two terms in Equation (23) cannot be approximated accurately with a difference formulation. Instead they can be summed to give $-\Delta M \int_{T_l^i}^{T_s^i} c_s \mathrm{d}T$. Substituting and rearranging gives

$$M_l^f c_l \Delta T_l + M_s^f c_s \Delta T_s = \left[L_m|_{T_l^i} + \int_{T_l^i}^{T_s^i} c_s \mathrm{d}T \right] \Delta M \tag{24}$$

Assuming $\rho_l = \rho_s = \rho$, we know that $M_l^f = \rho F_l^f V$, $M_s^f = \rho F_s^f V$, and $\Delta M = \rho \Delta F_s V$. Substituting and dividing by ρV leads to

$$F_l^f c_l \Delta T_l + F_s^f c_s \Delta T_s = \left[L_m|_{T_l^i} + \int_{T_l^i}^{T_s^i} c_s \mathrm{d}T \right] \Delta F_s \tag{25}$$

This is again underdetermined, so we assume a phase volume fraction weighted energy distribution, leading to

$$c_l \Delta T_l = \left[L_m|_{T_l^i} + \int_{T_l^i}^{T_s^i} c_s \mathrm{d}T \right] \Delta F_s \tag{26}$$

$$c_s \Delta T_s = \left[L_m|_{T_l^i} + \int_{T_l^i}^{T_s^i} c_s \mathrm{d}T \right] \Delta F_s \tag{27}$$

For time steps and shells in which no phase is initiated or terminated, we use Equations (26) and (27) to solve efficiently for the new phase temperatures. For time steps in which a phase is initiated or terminated, they are undefined and we must use Equation (19).

2.2.3. *Inter-Phase Heat Transport*

For a shell volume in which inter-phase transport is the only source (or sink) of energy to either phase, inter-phase heat transport can be represented by setting the change in enthalpy in each phase equal to inter-phase conductive heat transport, giving

$$F_l \rho_l c_l \frac{\partial T_l}{\partial t} = -h_{\mathrm{int}} A_v (T_l - T_s) \tag{28}$$

$$F_s \rho_s c_s \frac{\partial T_s}{\partial t} = -h_{\mathrm{int}} A_v (T_s - T_l) \tag{29}$$

The inter-phase heat transfer coefficient is modeled as $h_{\mathrm{int}} = \kappa_{\mathrm{int}}/\delta$, where δ is the length scale of transport, for which we use the dendrite tip radius. For free dendritic crystal growth, this radius is $\delta = 2D_{ww}\mathrm{Pe}/v$ (Caroli and Müller-Krumbhaar, 1995; Libbrecht and Tanusheva, 1999). D_{ww} is the self-diffusivity of water in liquid water and v is the growth speed. Pe is the Peclet number, determined for dendritic growth as

$$\mathrm{Pe}\, e^{\mathrm{Pe}} \int_{\mathrm{Pe}}^{\infty} \frac{e^{-\zeta}}{\zeta} d\zeta = \frac{c_p \Delta T_{\mathrm{int}}}{L_m} \tag{30}$$

where ζ is a dummy variable.

2.2.4. *Inter-Phase Solute Mass Transport*

During freezing, solute is segregated at the solid-liquid interface. A solute mass balance over the freezing shell takes the simple form,

$$M_{x,l}^i + M_{x,s}^i = M_{x,l}^f + M_{x,s}^f \tag{31}$$

where M_x refers here to the mass of solute. The other subscripts and superscripts have the same meanings as in Equation (18). We assume that partitioning at the interface can be described by the solid-liquid equilibrium distribution coefficient.

Then for a small volume of the shell frozen, $\Delta F_s V$, originally liquid water with solute concentration C_l^i, the solute mass in the ice formed will be $H_{sl} C_l^i \Delta F_s V$. This assumption is valid for Δt small enough that concentrations in the liquid phase do not build significantly. Then for our shell,

$$M_{x,s}^f = M_{x,s}^i + H_{sl} C_l^i \Delta F_s V \tag{32}$$

Combining this with Equation (31) and noting that $M = CFV$ leads to

$$C_s^f F_s^f - C_s^i F_s^i = H_{sl} C_l^i \Delta F_s \tag{33}$$

$$C_l^f F_l^f - C_l^i F_l^i = -H_{sl} C_l^i \Delta F_s \tag{34}$$

Dividing by the time step and taking the limit as Δt goes to zero, gives

$$\frac{dF_s C_s}{dt} = -\frac{dF_l C_l}{dt} = H_{sl} C_l^i \frac{dF_s}{dt} \tag{35}$$

Studies of dendritic crystal growth in solution (e.g. Harrison and Tiller, 1963; Tiller, 1964; Eddie and Kirwan 1973; Myerson and Kirwan, 1977a,b) indicate that equilibrium partitioning of solutes between phases can be significantly enhanced as dendrite branches grow together and trap solute-containing liquid pockets. As crystallization continues, there is no liquid pathway for solute transport out of the immediate environment. Hence, liquid-phase solute concentrations can increase drastically as the liquid pockets continue to freeze. When the pocket freezes completely, the trapped solute remains locally in the solid phase (minus solid-phase diffusion losses). To represent trapping during freezing, shells that freeze completely during any one time step retain all of the solute that was in the liquid phase at the beginning of the time step.

For melting, we allow all the solute originally in the ice volume melted, $\Delta F_s V$, to be transferred to the liquid phase (i.e. there is no segregation during melting). This gives

$$\frac{dF_s C_s}{dt} = -\frac{dF_l C_l}{dt} = C_s^i \frac{dF_s}{dt} \tag{36}$$

3. Computational Development

To numerically simulate partitioning of chemical solutes during freezing, we must consider issues of computational efficiency, computational process flow, and model conservation properties. Here we discuss our computational design.

3.1. PROCESS TIME SCALES AND TIME STEPS

Partitioning of chemical solutes during freezing is a complicated multi-process phenomenon. To develop a method for solving the process equations, we can compare the process time scales, or critical time steps.

Freezing and latent heat transport. Solidification is limited by the sensible heat released during freezing (the latent heat of fusion). If the time step is too large, temperatures will significantly exceed the equilibrium freezing temperature (which is not physically realistic) and the approximations used to develop Equation (25) will not be valid. To ensure a small critical temperature change, ΔT_c, we can approximate the critical time step, Δt_c, by rearranging Equation (26) or (27) (assuming liquid water and ice are initially at the same temperature), giving

$$\Delta t_c = \frac{c_p \Delta T_c}{L_m \Delta F_s / \Delta t_c} \tag{37}$$

where c_p is the heat capacity of the phase of interest. Substituting for $\Delta F_s / \Delta t_c$ (with Equation 17) and $A_v = 1/\Delta r$, we find

$$\Delta t_c = \frac{c_p \Delta T_c \Delta r}{L_m b_1 (\Delta T_{\text{int}})^{b_2}} \tag{38}$$

The critical time step is a function of the interfacial supercooling, the critical temperature change, and the grid shell spacing. Using values of $\Delta r = 0.01$ cm, $\Delta T_c = 0.1\,^\circ$C, and $1 < \Delta T_{\text{int}} < 40\,^\circ$C, the critical time step ranges from about 1×10^{-5} to 1×10^{-9} s.

Subgrid inter-phase transport. For inter-phase heat transport, we require that the change in temperatures of water and ice cannot be greater than a fraction ($E < 1$) of the initial difference between them. Using Equation (28), this criterion can be expressed as

$$E|T_l - T_s| \geq \text{maximum}\left[\left|\frac{\Delta t_c h_{\text{int}} A_v (T_l - T_s)}{\rho_s c_s F_s}\right|, \left|\frac{\Delta t_c h_{\text{int}} A_v (T_l - T_s)}{\rho_l c_l F_l}\right|\right] \tag{39}$$

Solving for Δt_c, results in

$$\Delta t_c = \text{minimum}\left[E\frac{\rho_s c_s F_s \Delta r}{h_{\text{int}}}, E\frac{\rho_l c_l F_l \Delta r}{h_{\text{int}}}\right] \tag{40}$$

The critical time step is a function of the volume fraction of ice. For $E = 0.1$ and $F_s = F_l = 0.5$, the critical time step is about 1×10^{-4} s. Note that there is no critical time step for inter-phase solute transport. It is an equilibrium process, converted to a time-dependent calculation using dF_s/dt.

Radial transport. For radial heat transport, we require that the change in temperature is not greater than a fraction of the difference in temperatures between two adjacent cells. Using Equations (5) and (6), this criterion results in

$$\Delta t_c = \text{minimum}\left[E\frac{\rho c_p (\Delta r)^2}{\kappa}\right] \tag{41}$$

where ρ and κ are the density and thermal conductivity of the phase of interest. Hence, the critical time step depends on gridspacing. For $\Delta r = 0.01$ cm and $E = 0.1$, it is about 1×10^{-3} s.

For radial solute mass transport, we use the same criterion for concentration as for temperature above. From Equations (7) and (8), we find

$$\Delta t_c = \text{minimum}\left[E\frac{(\Delta r)^2}{D}\right] \tag{42}$$

Again, the critical time step is again a function of gridspacing. For $\Delta r = 0.01$ cm and $E = 0.1$, the critical time step is about 1 s.

Since the critical time steps for distinct processes are orders of magnitude different, it is not necessary nor numerically efficient to calculate all processes at the smallest critical time step. Hence, the processes are time split and each is calculated separately in a serial manner. Additionally, since the critical time steps for freezing with latent heat transport and inter-phase heat transport depend on model variables that change significantly (ΔT_{int} and F_s, respectively), we use an adaptive time step for these processes.

3.2. ENTHALPY AND MASS CONSERVATION

To ensure physically realistic rates of freezing, numerical enthalpy losses or gains must be orders of magnitude smaller than losses to the hydrometeor particle environment. Enthalpy conservation in the model is calculated as

$$\frac{\Delta H_{\text{tot}}}{\Delta t} = 4\pi \sum_{j=1}^{N_s} r_j^2 \Delta r \frac{\Delta\left(F_s\rho_s \int_{T_b}^{T_s} c_s \mathrm{d}T + F_l\rho_l\left[L_m|_{T_l} + \int_{T_b}^{T_l} c_s \mathrm{d}T\right]\right)_j}{\Delta t}$$
$$+ 4\pi R^2\left(\kappa_s \frac{\Delta T_s}{\Delta r} + \kappa_l \frac{\Delta T_l}{\Delta r}\right) = 0 \tag{43}$$

where the first term represents the total enthalpy in the hydrometeor particle and the second term represents the loss/gain of enthalpy to the environment (via all the processes represented in Equations (11) and (12)). N_s is the total number of grid shells.

Non-physical enthalpy losses or gains can occur in model calculations during the processes of latent heat transport during freezing and sub-grid inter-phase heat transport. Equations (19) and (25) are used to calculate latent heat transport. Equation (19) is also used as an enthalpy balance to calculate enthalpy-conserving final liquid water temperatures for inter-phase heat transport, after an adaptive time-step loop using Equations (28) and (29). Since Equation (19) involves integrals whose limits are the unknowns, it is solved with an iterative convergence loop. Enthalpy conservation depends on the degree of convergence specified. We use convergence criteria (i.e. error tolerances) of 1×10^{-7} and 1×10^{-6} (in terms of the ratio of numerical enthalpy loss/gain to the total enthalpy in a shell), for latent heat transport and inter-phase heat transport, respectively. The enthalpy conservation properties of Equation (25) depend on the change in temperature during any given time step. The use of a threshold temperature change of 0.1 °C in the adaptive

time step solution of freezing (Equation (17)) ensures enthalpy conservation for Equation (25). It also ensures that freezing and the concurrent release of latent heat do not cause non-physical interfacial temperatures that significantly overshoot the equilibrium freezing temperature, once it is reached. These tolerances were chosen to ensure that the enthalpy loss/gain for each process module is more than two orders of magnitude less than the enthalpy loss to the environment, through repeated experimental model runs for a hydrometeor particle with no convective enhancement to heat transport in air. Strictly speaking, this enthalpy conservation criterion cannot be met for very early times, prior to the drop heating significantly. At early times, the energy loss to the environment is very close to zero. However, over the entire model simulation, enthalpy conservation is excellent.

The model equations are exactly mass conserving. Hence, conservation of solute and water mass is expected if there is no numerical error. As a benchmark of the model's performance, the conservation of solute mass is calculated as

$$\frac{\Delta M_{x,\mathrm{tot}}}{\Delta t} = 4\pi \sum_{j=1}^{N_s} r_j^2 \Delta r \frac{\Delta (F_s C_s + F_l C_l)_j}{\Delta t} + 4\pi R^2 \left(D_s \frac{\Delta C_s}{\Delta r} + D_l \frac{\Delta C_l}{\Delta r} \right) = 0 \tag{44}$$

where $M_{x,\mathrm{tot}}$ is the total mass of solute (in all phases) in the system. It is the sum of solute mass in the hydrometeor particle and solute mass losses from the particle to the environment.

The water mass balance is further simplified, as water mass is held constant in the model (i.e., there is no explicit representation of water mass transport). Hence, to benchmark the model's performance, water mass conservation is calculated as a simple sum of mass over all shells:

$$\frac{\Delta M_{\mathrm{tot}}}{\Delta t} = 4\pi \sum_{j=1}^{N_s} r_j^2 \Delta r \frac{\Delta (F_s \rho_s + F_l \rho_l)_j}{\Delta t} = 0 \tag{45}$$

where M_{tot} is the total mass of water (in both the liquid and solid phases) in the freezing hydrometeor particle. Note that although we account for heat loss due to evaporation and sublimation in Equations (11) and (12), as these may be important drivers for freezing, all other calculations assume constant water mass (in other words heat transport is decoupled from water mass transport). The implications of this representation are discussed in Section 5.

3.3. SOLUTION PROCEDURE

Figure 4 illustrates the process flow diagram of the model. A simulation is initiated by specifying ambient conditions (constant temperature and pressure), hydrometeor characteristics (initial drop and ice substrate sizes, temperatures, and air speed),

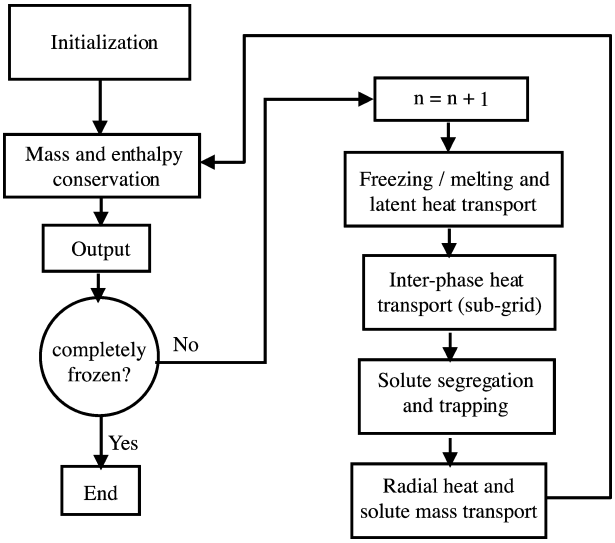

Figure 4. Flow diagram of model calculation modules. n is the outer-model time step.

solute concentrations in all phases, and computational parameters (Δt and N_s). The grid is determined and initialized by assuming the drop water is spread evenly around the ice substrate. Model constants (e.g., water density, hydrometeor particle fall speed, and ventilation coefficients) and temperature-dependent secondary model variables (e.g. latent heats of phase change, specific heats, conductivities, and diffusivities) are then initialized. Table I provides a list of model constants and variables, as well as references for the methods used for their calculation. Following initialization, the model time cycle of processes begins. For each outer-model time step, subgrid processes of phase change with latent heat transport, inter-phase heat transport, and solute segregation and trapping are calculated using individual time steps, as needed. The grid-resolved processes are then calculated at the outer-model time step. A second order central difference approximation is used for spatial discretization and time progression is discretized using a forward Euler formulation. After each outer-model time step (and at initialization), values of system enthalpy and mass are calculated. The simulation terminates when the hydrometeor particle is completely frozen. A detailed description of the model numerics can be found in Stuart (2002). Further explanation of the computational modeling terminology and methods used can be found in numerical modeling texts (e.g. Ferziger, 1998; Jacobson, 1999).

4. Model Simulations

To test and demonstrate the model, we simulated freezing and solute transport for several cases.

Table I. Model constants, variables, and solute properties[†]

Constants	Notation	Method source
Partial pressure of water vapor in air	p_a	See caption text
Thermal conductivity of moist air	κ_a	Pruppacher and Klett (1997, p. 508)
Diffusivity of water vapor in air	D_v	Pruppacher and Klett (1997, p. 503)
Density of condensed water	ρ_l, ρ_s	Pruppacher and Klett (1997, p. 87)
Ventilation coefficients for heat, water vapor, and solute transport in air	G_h, G_m	Pruppacher and Klett (1997, p. 541)
Variables	**Notation**	**Method source**
Latent heat of water sublimation	L_s	Jacobson (1999, p. 31)
Latent heat of water evaporation	L_e	Jacobson (1999, p. 31)
Latent heat of water fusion	L_m	See caption text
Saturation vapor pressure:		
Over liquid water	$P_{\text{sat}}^{v,l}$	Jacobson (1999, p. 33)
Over ice	$P_{\text{sat}}^{v,s}$	Jacobson (1999, p. 34)
Specific heat of liquid water	c_l	Pruppacher and Klett (1997, p. 93)
Specific heat of ice	c_s	Pruppacher and Klett (1997, p. 86)
Thermal conductivity of liquid	κ_l	Bird *et al.* (1960, p. 248)
Thermal conductivity of solid	κ_s	Pruppacher and Klett (1997, p. 676)
Solute properties	**Notation**	**Value used**
Henrys constant (−)	H_{lg}	Demonstration case: 28 Additional cases: 18000
Solid-liquid distribution coefficient (−)	H_{sl}	Demonstration case: 0 Additional cases: 1×10^{-6}
Diffusivity in air (cm^2/s)	D_g	Demonstration case: 0.1 Additional cases: 0.16
Diffusivity in liquid water (cm^2/s)	D_l	Demonstration case: 1×10^{-5} Additional cases: 7.7×10^{-6}
Diffusivity in ice (cm^2/s)	D_s	All cases: 1×10^{-10}

[†]*Constants* are calculated from the initial freezing conditions, i.e., ambient pressure, temperatures, and drop and substrate sizes. We assume the air is saturated with respect to liquid at the air temperature. The density of water and ice are assumed equal. For ventilation coefficients, the terminal fall speed was calculated as described in Jacobson (1999, p. 528). *Variables* vary in time and space, depending on the temperature. For enthalpy conservation, the latent heat of fusion is calculated as $L_{m(0)} + \int_0^T c_l - c_s$, where T is the temperature, and $L_{m(0)}$ was taken from Perry *et al.* (1984, pp. 3–120)). For thermal conductivity of liquid water, we used a linear regression on the data. *Solute properties* were assumed constant and are for hypothetical tracers. For the demonstration case, they are arbitrary with order of magnitude typical diffusivity values in the given phases. For the additional cases, we used rough estimates of values intended to be somewhat representative of SO_2. The effective Henrys constant accounts for S(IV) dissociation equilibria, as described in Seinfeld and Pandis (1997, p. 340–361), with necessary equilibrium constant and enthalpy data from this same source and Pruppacher and Klett (1997, pp. 748–749). A pH of 4.0 and a temperature of 0 °C were used. 2) The ice-water distribution coefficient is an assumed value, chosen to be greater than zero but an order of magnitude less than measured effective distribution coefficients discussed in Hobbs, (1974, p. 600–602). 3) Diffusivities in air and water were estimated as described in Lyman *et al.* (1990) and Jacobson (1999), assuming an air temperature of −10 °C and water temperature of 0 °C. The diffusivity in ice was left as the typical phase value.

4.1. DESCRIPTION OF THE DEMONSTRATION CASE

We simulated the freezing of a hydrometeor particle falling at its terminal fall speed, nucleated due to the impact of a supercooled drop 1000 μm in radius with an accretion substrate of 100 μm in radius. The air and supercooled drop temperatures were $-10\,^{\circ}$C. The ice substrate temperature was $-5\,^{\circ}$C. Ambient pressure was 300 hPa. A hypothetical chemical solute was used with properties listed in Table I. Solute concentrations in the gas-phase and supercooled drop were initially at equilibrium, with values 7×10^{-7} g/cm^3 and 2×10^{-5} g/cm^3, respectively. Initial solute concentration in ice was 0. The number of radial grid shells was 10, resulting in Δr of 1×10^{-2} cm. The outer model time step was 1×10^{-4} s.

4.2. DEMONSTRATION CASE RESULTS

Figure 5 shows the dynamics of freezing and temperature changes in the liquid water and ice phases. The progression in time and radial space of the fraction solid (a), liquid water temperature (b), and ice temperature (c) are shown. As seen in Figure 5a, the hydrometeor particle is initially liquid with a solid core (the original ice substrate). By 1×10^{-4} s, freezing begins to propagate out from the core of the hydrometeor particle, with the ice fraction values near the core increasing to about 0.1, and temperatures increasing near the core by up to three and five degrees in ice and liquid water, respectively. The temperature of ice in the core increases slightly (less than 1/10 of a degree). As time progresses, freezing propagates out to the boundary of the hydrometeor particle and the temperatures in ice and liquid water increase. By 9×10^{-4} s, ice has propagated radially throughout the hydrometeor particle. Due to the latent heat of fusion, temperatures quickly increase from the inside of the hydrometeor particle to the outside. By 1.6×10^{-3} s, liquid water temperatures throughout the two-phase zone are approximately uniform at about 272 K. Ice temperatures in the two-phase zone also increase, until they reach approximately equal values of 273 K at 1.1×10^{-3} s.

Once temperatures in the the two-phase zone are about equal, the ice fraction and temperatures increase more slowly and approximately uniformly. At 4.1×10^{-3} s, the ice fraction near the air boundary surpasses that in the interior, due to heat loss to the surrounding air. The temperature of the solid core (the ice substrate) increases slowly due to radial heat transport from the two-phase zone, but does not reach the temperature of the two-phase zone, 273.1 K, until about 3.3×10^{-2} s. As freezing progresses, temperatures approach the equilibrium freezing temperature of water. Far from the air boundary, temperatures reach 273.15 K at approximately 0.1 s. Temperatures near the surface are slightly depressed, due to heat loss to surrounding air which is at 263.15 K. In the first 7 seconds, the ice fraction near the air boundary increases significantly, while that in areas far from the boundary increase much less. At 7 seconds, a frozen shell forms at the particle-air boundary and freezing propagates inward until the entire hydrometeor particle is frozen at 24.6 s.

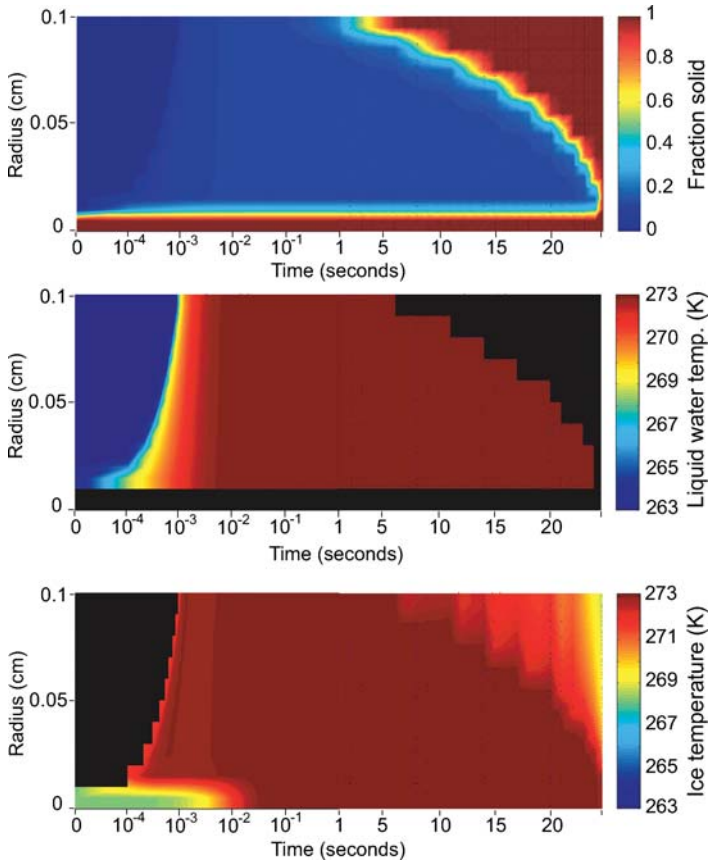

Figure 5. Radial profiles of fraction solid (a), liquid water temperature (b), and ice temperature (c) with time. Note that the scale of the time axis changes from logarithmic to linear at 1 second. Black indicates the value is undefined (because the phase does not exist at that point).

Concurrently, ice temperatures decrease from the outside in, due to heat transport to the surrounding air. However, temperatures do not decrease monotonically, likely due to the latent heat of fusion. Temperatures in liquid water also decrease from outside in, but as freezing progresses to completion in each shell, the liquid water temperature becomes undefined, and, hence, the profiles are shorter.

The progression of freezing seen in the model is both qualitatively and quantitatively consistent with experimental and theoretical studies of drop freezing. Previous work (e.g. Pruppacher and Klett, 1997; Macklin and Payne, 1967) indicates that nucleated drops freeze in approximately two stages. The first stage is termed the adiabatic stage. During this stage, ice propagates out from the nucleation site and the drop heats up to the equilibrium freezing temperature of water with relatively little heat loss to the drop environment (i.e. to air or the ice substrate). This stage is very quick, orders of magnitude faster than freezing of the

entire drop. The second stage is sometimes termed the diabatic stage. During this stage, freezing occurs more slowly and is limited by the rate of heat loss to the ice substrate and surrounding air. Our model results are qualitatively consistent with this progression.

Quantitative comparisons also support our model results. We can approximately bound the simulated adiabatic freezing time by two limits: 1) the time is takes for freezing to propagate through the drop (approximately 0.001 s) and 2) the time it takes the two-phase zone to heat to approximately the equilibrium freezing temperature (about 0.1 s). We use these bounds because freezing does not occur in exactly two stages. There is some heat loss to air and the ice substrate during the 'adiabatic' stage, and hence, the two-phase zone never completely reaches 273.15 K. During this stage, approximately 13% of the original supercooled drop mass froze in our simulation. This is consistent with drop freezing theory, which suggests that $c_l \Delta T / L_m$, or 13%, of the drop mass would freeze during the adiabatic stage (Pruppacher and Klett, 1997, p. 675).

By balancing heat released by freezing with that dissipated to air, Pruppacher and Klett (1997, p. 677–679) developed a theoretical expression (p. 678, Eqn. 16–36), validated by laboratory observations, for the total freezing time of droplets falling freely in air. Freezing times calculated with this expression for drops of radii from 1 to 2000 μm vary by orders of magnitude (Stuart and Jacobson, 2003). Using this expression, we estimate the freezing time to be 19.4 s for a 1000 μm drop at $-10\,^{\circ}$C, freely falling in air at the same temperature and a pressure of 300 hPa. This is in good agreement (within about 20%) with our simulated freezing time of 24.6 s.

Figure 6a and b show the progression of solute concentrations in the liquid water and ice phases, respectively, during freezing. Solute concentrations in liquid water were initially 2×10^{-5} g/cm^3 throughout the hydrometeor particle except in the original ice substrate core. The initial solute concentration in the core ice was 0. As freezing propagates through the drop, solute concentrations in liquid water away from the air boundary increase slightly to 2.3×10^{-5} g/cm^3 at 1 second, due to exclusion of solute from the ice phase during freezing. Concentrations near the air boundary decrease slightly to 1.9×10^{-5} g/cm^3 at 1 second, due to solute mass transport to air. After an ice shell forms at the air-particle surface and shell freezing propagates inward, concentrations in liquid water near the inner boundary of the ice shell increase more dramatically to about 1×10^{-4} g/cm^3 (with some higher values) due to exclusion from the ice phase and the lack of a sink to the air.

In ice (Figure 6b), concentrations near the center of the hydrometeor particle jump from 0 to 7×10^{-9} g/cm^3 due to freeze trapping, directly after freezing initiation. Solute concentrations in ice near the core increase slightly above 0 (to 3×10^{-19} g/cm^3) due to radial intra-phase solute mass transport. As ice propagates through the hydrometeor particle, the concentrations in ice throughout also increase to very small values ($\ll 1 \times 10^{-9}$ g/cm^3) due to radial solute mass transport. When the ice shell forms, concentrations in ice near the air boundary jump to 9.4×10^{-8} g/cm^3,

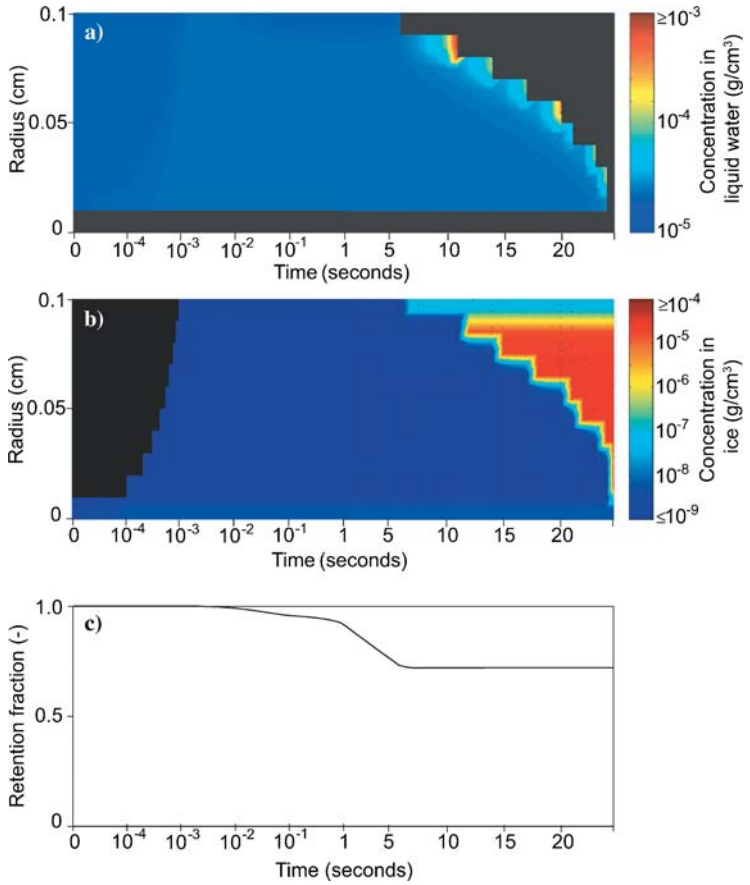

Figure 6. Radial profiles of solute concentration in liquid water (a), solute concentration in ice (b), and solute mass fraction retained in the hydrometeor particle (c) with time. Note that the scale of the time axis changes from logarithmic to linear at 1 second and that the color scales for concentration in liquid water and ice are different. Black indicates an undefined value.

due to freeze trapping. As freezing progresses inward, higher concentrations are trapped in ice due to higher concentrations in the liquid. In the area that freezes last, the concentrations in ice are slightly higher at 2.3×10^{-5} g/cm^3 than those in the original liquid water, due to redistribution (radial solute mass transport) during freezing. Very little mass is lost from the ice phase to air, since ice diffusivity is so small.

Figure 6c shows the total retention ratio (mass remaining over total original mass of solute) as a function of time. We see that in the first 0.1 seconds the retention ratio decreases precipitously from 1 to about 0.96 (note the logarithmic time axis scale). The retention ratio continues to decrease until an ice shell forms at the hydrometeor particle surface. Once a shell forms (at about 7 seconds), the retention ratio remains effectively constant at 0.72.

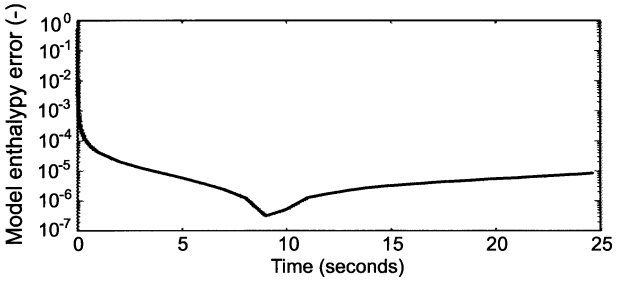

Figure 7. Absolute value of the model enthalpy error (cumulative numerical error over cumulative physical enthalpy loss to the hydrometeor particle surroundings) with time.

Since there are few data available on solute concentration distributions in frozen drops, the concentration results cannot be quantitatively compared with experimental data. However, the total retention ratio of 0.72 is within the range of measured retention ratios (∼0.01 to 0.83) for SO_2 (Iribarne *et al.*, 1983; Lamb and Blumenstein, 1987; Iribarne *et al.*, 1990; Iribarne and Barrie, 1995; Voisin *et al.*, 2000), which has somewhat similar chemical properties to our tracer solute. Additionally, the concentration distribution results are qualitatively consistent with concentration distributions observed in industrial freezing separation studies (e.g. see Zief and Wilcox, 1976; Pfann, 1966).

Finally, as benchmarks of our model success, we monitored the enthalpy and mass conservation during the simulation. Figure 7 shows the fractional model enthalpy error (cumulative computational enthalpy gain divided by the cumulative enthalpy loss to air). We use this metric because the energy loss to air drives the ultimate freezing of the hydrometeor particle; with too much computational enthalpy error, the drop would freeze either too slowly or too quickly. We see that enthalpy conservation is excellent in the simulation, with the final model enthalpy error approximately five orders of magnitude less than the total loss to the surroundings. Water and solute mass conservation are exact within the precision of our output values (9 significant digits).

4.3. ADDITIONAL CASE SIMULATIONS

We will discuss here model simulations for a few additional scenarios. The conditions of these cases were similar to the demonstration case, with a few exceptions. First, the ambient pressure was 700 hPa. Second, the air and drop temperatures were varied among the cases. Air and drop temperatures were -5, -10, and $-20\,^{\circ}$C for cases 1, 2, and 3, respectively. For all cases, the chemical tracer was based loosely on SO_2, with properties listed in Table I. Solute concentrations in the gas-phase and supercooled drop were initially at equilibrium, with values of 1.11×10^{-9} and 2.0×10^{-5} g/cm^3, respectively. Initial solute concentration in the ice substrate was 0.

For all cases, freezing occurred in a manner similar to that described for the demonstration case. The two-phase zone first heated to approximately 273 K after ice propagation throughout the drop. Ice shell formation occurred for cases 1 through 3 at 17, 8, and 4 s, respectively. Freezing subsequently occurred from the outside in, with the final freezing times for cases 1 through 3 of 59.6, 30.2, and 14.7 s, respectively. These freezing times are all within 20% of theoretical bulk freezing times (49.7, 25.4, and 12.5 s, respectively) estimated with the Pruppacher and Klett (1997) expression. The mass and energy balances for all cases were excellent, with an exact solute and water mass balance and enthalpy balance error (error / heat out) of less than 2×10^{-5} for all cases.

Solute concentrations in liquid water and ice also progressed in a manner similar to the demonstration case. However, due to a finite H_{sl} for these cases (as opposed to $H_{sl} = 0$ for the demonstration case), the concentrations in ice increased to about 2.1×10^{-11} g/cm^3 throughout the two-phase zone once freezing had propagated throughout the drop. The total retention ratio for all cases was approximately equivalent to the demonstration case.

We were surprised by this result because the air and supercooled drop temperatures varied between the cases. We expected to see higher retention ratios with decreasing temperature as has been found in some experimental studies (Lamb and Blumenstein,1987; Iribarne *et al.*, 1990; Snider *et al.*, 1992), and as is predicted by time scaling theory (e.g. Lamb and Blumenstein, 1987; Iribarne *et al.*, 1990; Snider *et al.*, 1992; Stuart and Jacobson, 2003). (Note that the solute properties were all equivalent and constant for the cases simulated here. Hence only the freezing and heat transfer processes were directly affected by the temperature change). In the simulations, we used a solute diffusivity in ice typical of transport through a monocrystalline solid. Hence, solute loss after ice shell formation is minimal and we are effectively representing a scenario in which ice shell formation, rather than complete freezing, controls the retention ratio. The relative importance to determining effective partitioning, of ice shell formation (adiabatic freezing control) versus complete freezing of the drop (diabatic freezing control) is an open question in the above literature. Since we are representing adiabatic freezing control in our simulations, we expected that the shorter ice shell formation times for the lower temperature cases would lead to higher retention ratios, in accordance with time scaling theory. Our equivalent simulated retention ratio results suggest that a compensating effect may not be accounted for in the current theory. A possible unrepresented compensating effect is the impact of freezing on the driving force for solute mass transport. Prior to ice shell formation, a driving force for solute transport out of the hydrometeor only exists when water freezes and, hence, increases solute concentrations in liquid water above the gas-liquid equilibrium value. This suggested effect is supported by the fact that the lower temperature cases underwent more volume freezing prior to shell formation. This may have counteracted the effect of decreased shell formation times on the retention ratio. Further work is needed to determine the importance of impacts of freezing

on the solute mass transport driving force, and ultimately on effective partitioning during freezing.

Additionally, this result may suggest the importance of the second stage of freezing to determining effective partitioning of solutes. Since we do not see a temperature dependence in our results, which represent adiabatic freezing control, loss during the second stage of freezing may be important to determining effective partitioning and its observed temperature dependence (though not necessarily under all freezing conditions). After the adiabatic freezing stage, loss from the hydrometeor may not always be controlled by diffusive loss through the ice crystal. Ice shell formation can be incomplete and fissures can form due to pressure buildup and cracking of the shell (e.g., Griggs and Choularton, 1983). These could provide a mechanism for solute loss at higher rates through water channels. Additionally, diffusion at grain boundaries may occur in polycrystalline ice (Huthwelker *et al.*, 2001), enhancing transport rates through ice. Further investigations of the importance of solute loss during the second stage of freezing, through the use of effective ice diffusivities (as discussed in Section 5), is needed.

5. Discussion

The model described here is a sophisticated representation of the multiple coupled processes occurring to influence the partitioning of chemical solutes during the freezing of a supercooled hydrometeor particle. It is also the first numerical model of this phenomenon. Nonetheless, many assumptions and simplifications were necessary in the development. These uncertainties and their implications are discussed here.

5.1. THE FREEZING REPRESENTATION

Assumptions and simplifications that may affect the simulated representation of freezing dynamics include the assumed value of the specific interfacial area A_v, the use of a grid-spacing-dependent parameterization of dendrite propagation, the use of a single spatial dimension, and the lack of an explicit representation of water mass transport.

The specific interfacial area directly affects the rate of freezing, as well as interphase heat and solute mass transport. We selected $1/\Delta r$ because this is the ratio of the shell border surface area to the shell volume, which provides a best guess of the scale of A_v. A sensitivity analysis indicated that varying A_v by an order of magnitude does not significantly affect the simulated freezing or partitioning of solute.

To represent the initial propagation of ice dendrites through the supercooled liquid, we only allow ice to initially form in shells that have ice in an adjacent shell. This representation is artificially dependent on the grid spacing, potentially affecting the accuracy of simulated freezing times. A test simulation similar to case

3, but with the shell size reduced in half, resulted in the same total freezing time (14.7 s) as for case 3. Hence, we conclude that it does not likely significantly affect our results.

For a numerically tractable first model, we have used a one-dimensional representation. Due to friction effects, varied hydrometeor particle geometries, and non-symmetric air flow patterns around falling drops, freezing hydrometeor particles can have distinct non-spherical shapes and non-symmetric heat transport rates from the particle surface. One potential effect of these non-isotropic phenomena, which has been observed in the laboratory (Griggs and Choularton, 1983), is freezing of ice from a single side or two sides of the hydrometeor particle. This could lead to non-isotropic liquid-phase transport pathways. Additionally, due to the one-dimensionality of our model, we must assume that ice nucleation occurs at the center of the drop. Recent studies indicate significant ice nucleation may occur at the drop surface by either preferential surface nucleation (Tabazadeh *et al.*, 2002) or evaporative freezing (Jacobson, 2003). We cannot represent the effects of these two- and three-dimensional phenomena. However, based on our model results we can hypothesize that the location of nucleation will not have a significant impact on overall individual hydrometeor particle freezing rates or on the effective partitioning of solutes. Our results indicate the even in the case of nucleation at the center of the hydrometeor particle (the farthest point from the surface of the drop), dendrites likely propagate rapidly enough to the surface of the drop to quickly form surface ice. Therefore, even in this case, heat loss to air controls potential ice shell formation and ultimate drop freezing, resulting in little impact of the ice nucleation site.

There is no explicit representation of water mass transport, such as fluid flow between shells or water loss/gain to the environment. In a one dimensional model, any such treatment would necessarily be very rudimentary and would necessitate significantly increased complexity in the computational method. Since we are specifically interested in freezing and solute partitioning, which are driven by heat transport and solute mass transport, respectively, we instead can treat the effects of water mass transport on these phenomena. This can be achieved through the use of ventilation coefficients in both the gas and liquid phases, leading to effective thermal conductivities and effective solute diffusivities. Terms in the heat transport and solute transport equations representing heat (and solute) loss via water evaporation and sublimation can also be used. Currently, we only treat the effects of ventilation in the gas phase, through the boundary conditions described in Section 2.1.3. Transport in the liquid phase is represented as being diffusive. Implementation of a parameterization for ventilation coefficients in the liquid phase, described in Stuart [2002], is planned in future work. However, good agreement between our simulated freezing times and previous work, indicates that liquid-phase ventilation effects may not be very important.

Continued developments in the freezing representation, such as the use of a dendrite initiation representation that accounts for dendrite tip travel distances or an expansion to a two- or three-dimensional model, may be useful for further

investigations of partitioning of solutes. However, we are quite confident in the freezing dynamics results of the current model, as simulated freezing physics, freezing times, and adiabatic freezing volumes compare very well to previous theoretical and experimental results.

5.2. THE CHEMICAL REPRESENTATION

For the chemical algorithm, additional uncertainties include the assumed values of the solid-liquid inter-phase distribution coefficient and the solute diffusivity in ice, the constant and equivalent water density assumption, the grid-spacing-dependent representation of solute trapping, and the lack of a chemical reaction representation.

The equilibrium solid-liquid solute distribution coefficient, H_{sl}, affects inter-phase solute mass transport (through Equation 35 in our model). Hence, its value may be important to the effective partitioning of chemical solutes during freezing. If equilibrium partitioning (as opposed to rate processes) controlled the effective partitioning, we would expect to see retention ratios equal to H_{sl} for a given solute. For the simulations here, we have used constant assumed values of H_{sl} (0 for the demonstration case and 1×10^{-6} for the additional cases). In actuality, the equilibrium solid-liquid distribution coefficient is a function of the concentration of solute in solution (e.g. Atkins, 1990), though for dilute enough systems, it is close to constant (e.g., Zief and Wilcox, 1976). Additionally, H_{sl} values for most dilute solutes in water are orders of magnitude less than 1 (Hobbs, 1974). Our simulations predict retention ratios significantly greater than the assumed values of H_{sl}. This suggests that rate processes (i.e. trapping) are more important than equilibrium partitioning to determining effective partitioning during freezing. It also indicates that the specific assumed values chosen as H_{sl} are not very important.

Solute diffusivities in hydrometeor ice are not well understood. Measured volume self-diffusivities of H and O in singe-crystalline ice are approximately 10^{-11} cm^2/s at $-10°C$ (Hobbs 1974). Measured diffusivities of other species (e.g. Diehl *et al.*, 1995; Sommerfeld *et al.*, 1998; Thibert and Domine, 1998) vary by a few orders of magnitude (from about 10^{-11} to 10^{-8} cm^2/s in these studies of HNO_3 and HCl). Differences appear to be affected by the degree of polycrystallinity, due to solute diffusion at ice crystal boundaries (Huthwelker *et al.*, 2001). Here, we use a assumed diffusivity in ice of 10^{-10} cm^2/s, which is near the lower end of measured values, and likely more representative of monocrystalline ice. This diffusivity resulted in minimal solute loss after ice shell formation, effectively representing a scenario in which ice shell formation, rather than complete freezing, controls the retention ratio. Investigations of the effects of greater solute diffusivities in ice are needed to understand the importance of the second stage of freezing on effective partitioning of solutes. This can be achieved in future work by varying the effective diffusivity of ice used in model simulations.

For tractability, we have assumed that the densities of liquid water and ice are constant and equivalent. Density differences can cause pressure gradients, cracking

of ice, and liquid water protrusions (Griggs and Choularton, 1983). This could allow preferential pathways of solute mass transport and loss to air. In a one-dimensional model, we cannot physically represent these phenomena. However, their potential effects could be represented through the use of an effective ice diffusivity, here ranging up to values representative of diffusivity in liquid water.

The amount of solute trapping in our model is artificially dependent on grid spacing, since we assume that all solute is trapped in ice when a grid shell freezes completely. A sensitivity simulation similar to case 3, but with Δr reduced in half, resulted in an overall retention ratio that was 18% higher than for case 3. Therefore, a more physical parameterization may be needed for further investigations of partitioning during freezing. A future improvement to the trapping representation will be the use of a rate-dependent effective solid-liquid distribution coefficient, H_{sl-eff} (in place of H_{sl}), instead of a separate trapping algorithm. Possible models for H_{sl-eff} include the Burton *et al.* (1953) and Myerson and Kirwan (1977a,b) models.

Finally, we do not currently represent chemical reactions, though experimental studies indicate that reactions may impact the effective partitioning of some chemicals during freezing (e.g., Iribarne and Barrie, 1995; Snider and Huang, 1998). A goal of our work is to consider the effects of reactions on the effective partitioning of chemical solutes (and the effects of the redistribution of solutes during freezing on reaction rates) by coupling a chemistry ordinary differential equation solver to our model. However, our current model only provides information on the impacts of physical processes on chemical fate.

Further improvements of the chemical algorithms in our model are needed for accurate prediction of partitioning of solutes during freezing. Nonetheless, results from our simulation cases, discussed in Section 4, indicate that the current model represents the redistribution of solute in a manner qualitatively consistent with previous work on freezing segregation in both industrial applications and in hydrometeor ice. It therefore provides a good basis for further development and for investigations of the redistribution and chemistry of trace chemicals in clouds.

6. Conclusions

We have developed and demonstrated a one-dimensional computational model of freezing and partitioning of chemical solutes in a hydrometeor particle. This provides a first computational model that resolves the multiple drop-scale processes governing the redistribution of chemical solutes during supercooled drop freezing. The simulated profiles of freezing fraction, temperature, and concentration are physically realistic and qualitatively consistent with previous theoretical and experimental work. Freezing times and adiabatic freezing volumes are also quantitatively consistent with those from previous work. Enthalpy and mass (of water and solute) conservation were excellent in all model simulations.

Findings include that ice shell formation is largely controlled by heat loss to air and not propagation of ice dendrites to the hydrometeor particle surface, and that

the location of ice nucleation is not likely very important to hydrometeor particle freezing times or the effective partitioning of solutes. Even in the case of nucleation at the center of the drop (as represented here), dendrites rapidly propagated to the surface and formed surface ice. Freezing then proceeded inward from the outside of the hydrometeor particle. The specific interfacial surface area was also not found to be a significant determinant of freezing or partitioning. Additionally, our retention ratio results indicate that trapping is more important to the effective partitioning of chemical solutes than solid-liquid equilibrium partitioning. Finally, we found equivalent effective partitioning results despite distinct freezing temperatures for the simulations here, which representing adiabatic freezing control. This suggests that the impacts of freezing on the driving force for mass transport may be important. It also suggests the potential importance of the second stage of freezing to determining observed retention ratios, though further work is need to test these implications.

Acknowledgements

We would like to thank the anonymous reviewers for their helpful comments. This work was supported by a U.S. Environmental Protection Agency STAR Graduate Fellowship (U915641). Partial support was also provided through grants from the National Science Foundation (grant numbers ATM9694118 and ATM0101596) and the National Aeronautics and Space Administration (grant number NAG5-8645).

References

Abbatt, J. P. D., 2003: Interactions of atmospheric trace gases with ice surfaces: Adsorption and reaction. *Chemical Reviews* **103**, 4783–4800.

Audiffren, N., Cautenet, S., and Chaumerliac, N., 1999: A modeling study of the influence of ice scavenging on the chemical composition of liquid-phase precipitation of a cumulonimbus cloud. *Journal of Applied Meteorology* **38**, 1148–1160.

Atkins, P. W., 1990: *Physical Chemistry*, 4th ed., Freeman, W. H. and Co., New York.

Barth, M. C., Stuart, A. L., and Skamarock, W. C., 2001: Numerical simulations of the July 10, 1996, Stratospheric-Tropospheric Experiment: Radiation, Aerosols, and Ozone (STERAO) - Deep Convection experiment storm: Redistribution of soluble tracers. *Journal of Geophysical Research* **106**(D12), 12381–12400.

Bird, R. B., Stewart, W. E., and Lightfoot, E. N., 1960: *Transport Phenomena*, John Wiley & Sons, Inc., New York.

Bolling, G. F. and Tiller, W. A., 1961: Growth from the Melt. III. Dendritic Growth. *Journal of Applied Physics* **32**(12), 2587–2605.

Burton, J. A., Prim, R. C., and Slichter, W. P., 1953: *Journal of Chemical Physics* **21**, 1987.

Caroli, B. and Muller-Krumbhaar, H., 1995: Recent advances in the theory of free dendritic growth. *ISIJ International* **35**(12), 1541–1550.

Chatfield, R. B. and Crutzen, P. J. 1984: Sulfur dioxide in remote oceanic air: Cloud transport of reactive precursors. *Journal of Geophysical Research* **89**(D5), 7111–7132.

Chen, J.-P. and Lamb, D., 1990: The role of precipitation microphysics in the selective filtration of air entering the upper troposphere. In. *1990 Conference on Cloud Physics*, pp. 479–484, Am. Meteorol. Soc., Boston, Mass.

Chen, J.-P. and Lamb, D., 1994: Simulation of cloud microphysical and chemical processes using a multicomponent framework. Part I: Description of the Microphysical Model. *Journal of the Atmospheric Sciences* **51**(18), 2613–2630.

Cho, H. R., Niewiadomski, M., and Iribarne, J., 1989: A model of the effect of cumulus clouds on the redistribution and transformation of pollutants. *Journal of Geophysical Research* **94**(D10), 12895–12910.

Clegg, S. M. and Abbatt, J. P. D., 2001: Oxidation of SO_2 by H_2O_2 on ice surfaces at 228 K: A sink for SO_2 in ice clouds. *Atmospheric Chemistry and Physics* **1**, 73–78.

Dickerson, R. R., Huffman, G. J., Luke, W. T., Nunnermacker, L. J., Pickering, K. E., Leslie, A. C. D., Lindsey, C. G., Slinn, W. G. N., Kelly, T. J., Daum, P. H., Delany, A. C., Greenberg, J. P., Zimmerman, P. R., Boatman, J. F., Ray, J. D., and Stedman, D. H., 1987: Thunderstorms: An important mechanism in the transport of air pollutants. *Science* **235**, 460–465.

Edie, D. D. and Kirwan, D. J., 1973: Impurity trapping during crystallization from melts. *Industrial Engineering and Chemistry. Fundamentals* **12**(1), 100–106.

Ferziger, J. H., 1998: *Numerical Methods for Engineering Application*, 2nd ed., John Wiley & Sons.

Griggs, D. J. and Choularton, T. W., 1983: Freezing modes of riming droplets with application to ice splinter production. *Quarterly Journal of the Royal Meteorological Society* **109**, 243–253.

Hales, J. M. and Dana, M. T., 1979: Precipitation scavenging of urban pollutants by convective storm systems. *J. Appl. Meteorol.* **18**(3), 294–316.

Harrison, J. D. and Tiller, W. A., 1963: Controlled freezing of water, in W. D. Kingery (ed.), *Ice and Snow: Properties, Processes, and Application*, M.I.T Press, Cambridge.

Hobbs, P. V., 1974: *Ice Physics*, Clarendon, Oxford, UK.

Huffman, W. A. and Snider, J. R., 2004: Ice-oxyhydrocarbon interactions in the troposphere. *Journal of Geophysical Research* **109**, D01302, doi:10.1029/2003JD003778.

Iribarne, J. V. and Barrie, L. A., 1995: The oxidation of S(IV) during riming by cloud droplets. *Journal of Atmospheric Chemistry* **21**, 97–114.

Iribarne, J. V., Barrie, L. A., and Iribarne, A., 1983: Effect of freezing on sulfur dioxide dissolved in supercooled droplets. *Atmospheric Environment* **17**(5), 1047–1050.

Iribarne, J. V. and Pyshnov, T., 1990: The effect of freezing on the composition of supercooled droplets – I. Retention of HCl, HNO_3, NH_3, and H_2O_2. *Atmospheric Environment* **24A**(2), 383–387.

Iribarne, J. V., Pyshnov, T., and Naik, B., 1990: The effect of freezing on the composition of supercooled droplets – II. Retention of S(IV). *Atmospheric Environment* **24A**(2), 389–398.

Jacobson, M. Z., 1999: *Fundamentals of Atmospheric Modeling*, Cambridge University Press.

Jacobson, M. Z., 2003: Development of mixed-phase clouds from multiple aerosol size distributions and the effect of the clouds on aerosol removal. *Journal of Geophysical Research* **108**(D8), 4245, doi:10.1029/2002JD002691.

Jaegle, L., Jacob, D. J., Wennberg, P. O., Spivakovsky, C. M., Hanisco, T. F., Lanzendorf, E. J., Hintsa, E. J., Fahey, D. W., Keim, E. R., Proffitt, M. H., Atlas, E. L., Flocke, F., Schauffler, S., McElroy, C. T., Midwinter, C., Pfister, L., and Wilson, J. C., 1997: Observed OH and HO_2 in the upper troposphere suggest a major source from convective injection of peroxides. *Geophysical Research Letters* **24**(24), 3181–3184.

Kreidenweis, S. M., Zhang, Y., and Taylor, G. R., 1997: The effects of clouds on aerosol and chemical species production and distribution 2. Chemistry model description and sensitivity analysis. *Journal of Geophysical Research* **102**(D20), 23867–23882.

Lamb, D. and Blumenstein, R., 1987: Measurement of the entrapment of sulfur dioxide by rime ice. *Atmospheric Environment* **21**(8), 1765–1772.

Libbrecht, K. G. and Tanusheva, V. M., 1999: Cloud chambers and crystal growth: effects of electrically enhanced diffusion on dendrite formation from neutral molecules. *Physical Review E* **59**(3), 3253–3261.

Logan, J. A., 1983: Nitrogen oxides in the troposphere: Global and regional budgets. *J. Geophys. Res.* **88**, 10785–10807.

Lyman, W. J., Reehl, W. F., and Rosenblatt, D. H., 1990: *Handbook of Chemical Property Estimation Methods*, American Chemical Society, Washington D.C.

Macklin, W. C. and Payne, G. S., 1967: A theoretical study of the ice accretion process. *Quarterly Journal of the Royal Meteorological Society* **93**, 195–213.

Mari, C., Jacob, D. J., and Bechtold, P., 2000: Transport and Scavenging of Soluble Gases in a Deep Convective Cloud. *Journal of Geophysical Research* **105**(D17), 22255–22267.

Mitchell, D. L. and D. Lamb, 1989: Influence of riming on the chemical composition of snow in winter orographic storms. *Journal of Geophysical Research* **94**(D12), 14831–14840.

Myerson, A. S. and Kirwan, D. J., 1977a: Impurity trapping during dendritic crystal growth. 1. Computer simulation. *Industrial Engineering and Chemistry. Fundamentals* **16**(4), 414–420.

Myerson, A. S. and Kirwan, D. J., 1977b: Impurity trapping during dendritic crystal growth. 2. Experimental results and correlation. *Industrial Engineering and Chemistry. Fundamentals* **16**(4), 420–425.

Pfann, W. G., 1966: *Zone Melting*, 310 pp., John Wiley & Sons, New York.

Perry, R. H., Green, D. W., and Maloney, J. O. (Eds.), 1984: *Perry's Chemical Engineers' Handbook*, 6th ed., McGraw-Hill Book Company, New York.

Pickering, K. E., Thompson, A. M., Scala,J. R., W.-K. Tao, Dickerson, R. R., and Simpson, J., 1992: Free tropospheric ozone production following entrainment of urban plumes into deep convection. *Journal of Geophysical Research* **97**(D16), 14985–18000.

Prather, M. J. and Jacob, D. J., 1997: A persistent imbalance in HOx and NOx photochemistry of the upper troposphere driven by deep tropical convection. *Geophysical Research Letters* **24**(24), 3189–3192.

Pruppacher, H. R. and Klett, J. D., 1997: *Microphysics of Clouds and Precipitation*, Kluwer Academic Publishers, Normwell, Mass., pp. 954.

Rutledge, S. A., Hegg, D. A., and Hobbs, P. V., 1986: A numerical model for sulfur and nitrogen scavenging in narrow cold-frontal rainbands 1. Model description and discussion of microphysical fields. *Journal of Geophysical Research* **91**(D13), 14385–14402.

Seinfeld, J. H. and Pandis, S. N., 1997: *Atmospheric Chemistry and Physics. From Air Pollution to Climate Change*, John Wiley & Sons, Inc., New York.

Sherwood, T. K., Pigford, R. L., and Wilke, C. R., 1975: *Mass Transfer*, McGraw-Hill Book Company, New York.

Snider, J. R. and Huang, J., 1998: Factors influencing the retention of hydrogen peroxide and molecular oxygen in rime ice. *Journal of Geophysical Research* **103**(D1), 1405–1415.

Snider, J. R., Montague, D. C., and Vali, G., 1992: Hydrogen peroxide retention in rime ice. *Journal of Geophysical Research* **97**(D7), 7569–7578.

Stuart, A. L., 2002: *Volatile Chemical Partitioning During Cloud Hydrometeor Freezing and its Effects on Tropospheric Chemical Distributions*. Ph.D thesis, Stanford University.

Stuart, A. L. and Jacobson, M. Z., 2003: A timescale investigation of volatile chemical retention during hydrometeor freezing: Nonrime freezing and dry growth riming without spreading. *J. Geophys. Res.* **108**(D6), 4178, doi:10.1029/2001JD001408.

Stuart, A. L. and Jacobson, M. Z., 2004: Chemical retention during dry growth riming. *J. Geophys. Res.* **109**, D07305, doi:10.1029/2003JD004197.

Tabazadeh, A., Djikaev, Y. S., and Reiss, H., 2002: Surface crystallization of supercooled water in clouds. *PNAS* **99**(25), 15873–15878.

Takenaka, N., Ueda, A., Daimon, T., Bandow, H., Dohmaru, T., and Maeda, Y., 1996: Acceleration mechanism of chemical reaction by freezing: The reaction of nitrous acid with dissolved oxygen. *Journal of Physical Chemistry* **100**, 13874–13884.

Tien, R. H. and Geiger, G. E., 1967: A heat-transfer analysis of the solidification of a binary eutectic system. *Journal of Heat Transfer* **89**(3), 230–234.

Voisin, D., Legrand, M., and Chaumerliac, N., 2000: Scavenging of acidic gases (HCOOH, CH3COOH, HNO3, HCl, and SO2) and ammonia in mixed liquid-solid water clouds at the Puy de Dome mountian (France). *Journal of Geophysical Research* **105**(D5), 6817–6835.

Wang, C. and Chang, J. S., 1993: A three-dimensional numerical model of cloud dynamics, microphysics, and chemistry 3. Redistribution of pollutants. *Journal of Geophysical Research* **98**(D9), 16787–16789.

Yin, Y., Carslaw, K. S., and Parker, D. J., 2002: Redistribution of trace gases by convective clouds—mixed-phase processes. *Atmospheric Chemistry and Physics* **2**, 293–306.

Zief, M. and Wilcox, W. R., 1967: *Fractional Solidification*, Marcel Dekker, New York, pp. 714.